Floquet π mode engineering in non-Hermitian waveguide lattices

Shengjie Wu,* Wange Song,* Shenglun Gao, Yuxin Chen, Shining Zhu, and Tao Li†

National Laboratory of Solid State Microstructures, Key Laboratory of Intelligent Optical Sensing and Manipulation, Jiangsu Key Laboratory of Artificial Functional Materials, College of Engineering and Applied Sciences, Nanjing University, Nanjing 210093, China and Collaborative Innovation Center of Advanced Microstructures, Nanjing 210093, China

(Received 8 February 2021; revised 31 March 2021; accepted 28 April 2021; published 15 June 2021)

Floquet topological systems exhibit rich physics associated with quasienergy band structures and new topological states; nevertheless, they are usually explored in Hermitian systems. Recent studies have shown the capability of non-Hermiticity in engineering topological states, while the interplay of Floquet topological phases and non-Hermiticity remains unclear. Here, we reveal that the non-Hermitian modulation can induce the phase transitions between trivial and nontrivial topological Floquet states. Our study theoretically predicts that the non-Hermitian modulation can create a Floquet π mode in an originally topological trivial system according to the reopening of quasienergy band gap (i.e., the π gap), which is well confirmed experimentally in the silicon waveguide platform. Our approach shows the powerful capability of non-Hermitian modulation in engineering topological modes in Floquet photonics systems and would inspire different possibilities in optical field manipulation in open systems.

DOI: 10.1103/PhysRevResearch.3.023211

Topological photonics, with gapped bulk energy spectrum and robust edge states within the band gap, have received considerable research interest. There have been a lot of works about topological protected photonic modes realized in various systems. Topological zero mode, as a particular kind of topological mode with energy pinned at zero in the simplest one-dimensional (1D) system, named the Su-Schrieffer-Heeger (SSH) model, received much attention due to its robustness against perturbations [1–8]. Recently, topological photonic configurations have been extended from static to periodically driven systems, known as Floquet topological photonics (FTP) [9–26]. The periodic driving enables more flexible modulation on optical modes, which leads to intriguing phenomena [15–28]. For example, the 1D Floquet SSH model can host a different kind of edge mode called the anomalous π mode, which differs from the zero mode in the SSH model and shows an oscillation behavior on the edge of lattice. This mode has been theoretically studied with Floquet theory and experimentally realized in microwave optical systems [22–25,27–30].

On the other hand, non-Hermitian systems with parity-time (PT) symmetry modulation have received great attention in the photonics, in which gain and loss can be introduced to control optical modes and light propagations [31–40]. Recently, the interplay of topology and non-Hermiticity has inspired explorations. For example, the non-Hermitian parameters can provide a powerful tool to modulate the nontrivial topological states, such as non-Hermitian topological phase [41–53], zero mode recovering [54], light steering [55], and the topological transport quantization [56]. Thus, it is of interest to investigate the Floquet engineering with the presence of non-Hermitian modulations.

Here, we theoretically and experimentally demonstrate a non-Hermiticity-induced Floquet π mode in a periodically driven SSH model. The interplay of non-Hermitian PT-symmetric gain/loss strength and the Floquet edge state is systematically investigated. By varying the gain-loss profile and Floquet modulation frequency, we construct a topological phase diagram to illustrate the topological phase transition and existence of topological states. It is found that the non-Hermiticity can open a nontrivial topological gap (i.e., π gap) in the quasienergy band and ensures the emergence of the π mode. We carried out the experiments in a silicon waveguides platform with controlled losses, which show good agreement with theoretical results. Our study reveals that the topological property of Floquet systems can be tuned by non-Hermitian parameters and implies photonic applications in non-Hermitian Floquet systems.

We start by considering a Floquet modulated PT-symmetric SSH model where the hopping terms are modulated as light propagates along the z direction in a waveguide array,

$$\mathrm{H} = \sum_{\mathrm{n}=1}^{N} \beta_0 a_n^\dagger a_n + \sum_{n=1}^{N} (-1)^n i\gamma a_n^\dagger a_n + \sum_{n=1}^{N-1} [c_0 + (-1)^n \delta(z)] a_n^\dagger a_{n+1} + \mathrm{H.c.}, \quad (1)$$

where β_0 is the effective propagation constant for a single waveguide and can be taken equal to a reference energy (zero energy). The second term on the right is the PT-symmetric

*These authors contributed equally to this work.
†Corresponding author: taoli@nju.edu.cn

Published by the American Physical Society under the terms of the Creative Commons Attribution 4.0 International license. Further distribution of this work must maintain attribution to the author(s) and the published article's title, journal citation, and DOI.

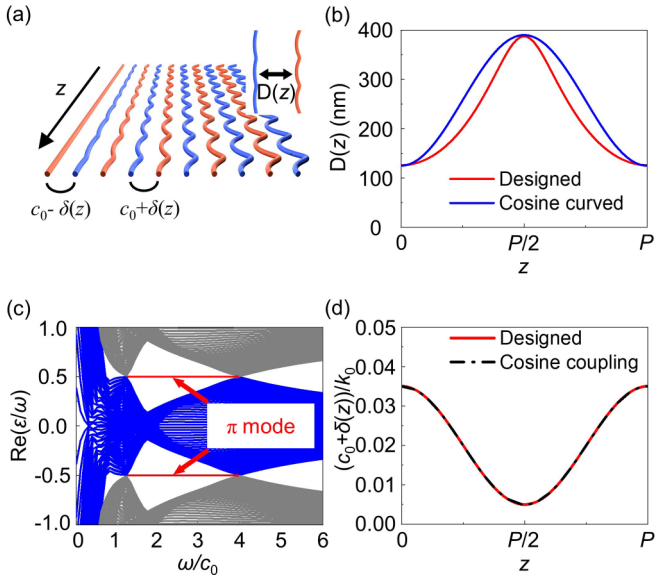

FIG. 1. (a) Schematic illustration of non-Hermitian periodically curved waveguide array, where the red and blue colors indicate the gain and loss respectively. The inset shows the scheme of the gap $D(z)$ between adjacent waveguides. (b) $D(z)$ as function of z in a full period under different waveguide profiles, where "Designed" corresponds to our inverse designed waveguide profile to meet the requirement of coupling strength $c_0 + \delta(z)$ and "Cosine curved" corresponds to widely used cosine function modulated waveguide. (c) Quasienergy spectrum under OBCs with 60 waveguides as a function of ω/c_0. (d) Coupling strength of $[c_0 + \delta(z)]/k_0$ of different waveguide profile, where "Cosine coupling" corresponds to the exact theoretical model with cosine function modulated coupling term. Our designed waveguide profile can exactly realize the cosine function modulated coupling as required by the Floquet model.

gain and loss with γ being the gain/loss strength, and the third term represents the coupling between nearest-neighbor waveguides where c_0 is the constant coupling coefficient. $\delta(z)$ is the Floquet modulated staggered coupling term and is defined as

$$\delta(z) = \delta_0 \cos(\omega z), \tag{2}$$

where δ_0 is the Floquet modulation strength and ω is the modulation frequency. Since the coupling strength of adjacent waveguides depends exponentially on the separation distance between two waveguides (see Appendix B), the coupling between cosine curved waveguides does not exactly satisfy cosine function modulation on coupling coefficients. Here, the waveguide profile is determined through an inverse design to make the coupling strength exactly match the cosine modulation. Figure 1(a) shows the waveguide scheme, which has a gradually increased bending profile. The designed gap of $c_0 + \delta(z)$ of adjacent waveguides is plotted as the red curve in Fig. 1(b), which clearly differs from the cosine (blue) curve. Rightly due to this special bending profile of waveguides, the deduced coupling strength can satisfy the cosine function modulation, as shown in Fig. 1(d).

According to the Floquet theory, a quasienergy band structure governed by a time-periodic Hamiltonian with period $P = 2\pi/\omega$ can be described in terms of so-called quasienergy ε, analogs of the eigenenergies in a static system. The corresponding Floquet states belong to the extended Hilbert space $R \otimes T$, which is a direct product of the usual Hilbert space R and the space T of periodic functions $e^{i(n\omega t)}$, where the index n defines a subspace called Floquet replica [23,25,28,29]. Previous research has pointed out that the π mode exists in a certain region of modulation frequency ω. The quasienergy band structure under open boundary conditions (OBCs) with 60 waveguides as a function of ω/c_0 is calculated with $\gamma = 0$, $c_0 = 0.02k_0$, and $\delta_0 = 0.015k_0$, where the k_0 is the wave vector in free space and taken to 1 in theoretical calculations [see Fig. 1(c)]. Blue bands correspond to $n = 0$ replica and gray bands correspond to $n = \pm 1$ replicas. The π modes are highlighted in red and it is clear that π modes only exist in the frequency region of $[4/3c_0,\ 4c_0]$. According to the periodic nature of quasienergy, we focus on the first Floquet Brillouin zone $(-\omega/2, \omega/2]$. A gap at $\varepsilon = \omega/2$ (thus called the π gap) occurs due to Floquet replica coupling. The topology of the π gap takes a transition whenever a new pair of replicas starts to contribute at the given midgap energy, and the Zak phase of such gap acquires a π shift [23]. The transition point depends on the bandwidth $\Delta = 4c_0$ and Floquet modulation frequency ω. The π gap with a nonzero Zak phase hosts the π mode at $\varepsilon = \omega/2$. At the high frequency region, the π gap is trivial because no replica touches $\varepsilon = \omega/2$. At $\omega = \Delta$, $n = 0$, and $n = 1$ replicas start to contribute to the gap with an emergence of the π mode. At $\omega = \Delta/3$, $n = 2$, and $n = -1$ replicas touch $\varepsilon = \omega/2$, which leads to the closing of the π gap and a phase transition from topological nontrivial to trivial.

In non-Hermitian photonics, strong gain/loss strength modulation can weaken the effective coupling among the waveguides and optical modes, which can lead to mode localization and recovery of zero modes in static systems [51]. However, the reemergence of the π mode here has a totally different mechanism. In the non-Hermitian SSH model, every replica band is modulated by gain and loss and the bandwidth becomes

$$\Delta = 2\sqrt{4c_0^2 - \gamma^2}. \tag{3}$$

According to Eq. (3), changing gain/loss strength can modify the bandwidth Δ. As a result, the topological transition of the π gap can be controlled by ω and γ. The modulation of ω on the quasiband structures has been well illustrated in Fig. 1(c) and also in former research [25]. Here, we mainly focus on the modulation of γ. We first consider a Floquet systems that is topologically trivial in the Hermitian case [e.g., $\omega = 1.33c_0$ according to Fig. 1(c)]. Interestingly, when adding the non-Hermiticity parameters, it can be tuned to a topologically nontrivial systems with the emergence of the π mode, as shown in Fig. 2(a), where the real part of the quasienergy spectrum under OBCs with 60 waveguides as a function of gain/loss strength γ is demonstrated (the imaginary part is shown in Appendix D). It is evident that the π modes can be recovered by certain amount of gain/loss (i.e., $\gamma > \gamma_c = 0.142c_0$) as a result of trivial-to-nontrivial topological transition. However, further increasing the non-Hermitian strength will transfer the system to a topological trivial one, thus making the π mode disappear. The topological property of the π gap can be described by the topological invariant G_π

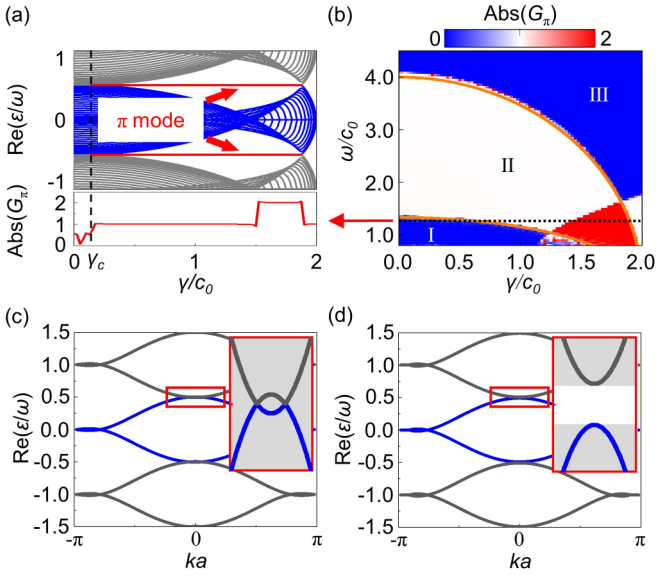

FIG. 2. (a) Real part of quasienergy spectrum under OBCs with 60 waveguides as a function of γ/c_0. $\gamma_c = 0.142c_0$ (marked by the black dashed line) is the threshold of gain/loss strength of recovering π mode. The π modes are highlighted in red. The bottom panel depicts the absolute value of numerically calculated G_π. (b) Calculated G_π and phase diagram of π mode as a function of γ/c_0 and ω/c_0. π mode exists in region II, and disappears in I and III. Orange lines indicate the boundary of different topological phases and the black dotted line indicates the trajectory of topological phase transition of increasing γ, corrsponding to (a). Quasienergy band under PBCs for a Hermitian $\gamma = 0$ (c) and non-Hermitian $\gamma = 0.005k_0$ (d) systems, respectively. k is the Bloch wave vector and a is the transverse period. Inset depicts the band structure near the π gap for better visualization. Here we set $c_0 = 0.02k_0$, $\delta_0 = 0.015k_0$, and $\omega = 1.33c_0$.

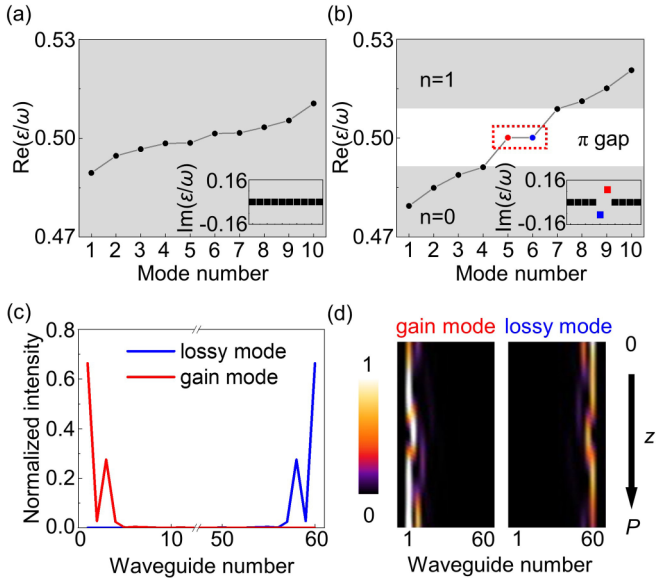

FIG. 3. (a), (b) Quasienergies of 60 waveguides in the Hermitian $\gamma = 0$ (a) and non-Hermitian $\gamma = 0.005$ (b) cases. Only ten quasienergies around the first Floquet Brillouin zone edge are shown. Inset shows the imaginary part of quasienergy. In the non-Hermitian system, π gap opens and a pair of π modes appear, including one lossy mode and one gain mode, corresponding to the blue and red modes in the inset in (b), respectively. (c) Normalized intensity at $z = 0$ of modes in the non-Hermitian cases [circled by red dotted line in (b)]. (d) The dynamic evolution of recovered π modes for 60 waveguides.

[24,25], which applies to Floquet systems, and a nontrivial π gap corresponding to nonzero G_π. The bottom panel in Fig. 2(a) depicts the absolute value of G_π with increasing γ, which clearly shows the topological transition induced by gain/loss. To more clearly and elaborately reveal the effect, we show in Fig. 2(b) a topological phase diagram based on G_π in the parametric space of ω and γ. Nontrivial π gap opens in regions II where the π mode appears, while regions I and III are in a topologically trivial phase without the π mode, and the boundaries between different topological phases are indicated by orange lines. The black dotted line indicates the trajectory of topological phase transition with $\omega = 1.33c_0$ by increasing γ, corresponding to the case analyzed in Fig. 2(a). Though G_π cannot describe the topological property precisely since induced gain/loss breaks the chiral symmetry [i.e., $\sigma_z H(z,k)\sigma_z \neq -H(-z,k)$], such as a noninteger value of G_π and the break of correspondence between G_π and π modes at the low-frequency and strong gain/loss region, it can indicate the topological transition on the whole. The non-Hermiticity-induced topological transition can be explained by analyzing the replica bands. The replica band of Hermitian ($\gamma = 0$) and non-Hermitian ($\gamma = 0.005k_0$) waveguide lattice was calculated at $\omega = 1.33c_0$ under periodic boundary conditions (PBCs), as shown in Figs. 2(c) and 2(d). The zoom-in band structure around $\varepsilon = \omega/2$ is also shown in the insets.

For $\gamma = 0$, $n = 0$, and $n = 1$ replicas touch and there is no π gap. However, when a certain amount of gain and loss ($\gamma = 0.005k_0$) are introduced, the $n = 0$ and $n = 1$ replicas are separated thus the π gap opens at $\varepsilon = \omega/2$ [see inset in Fig. 2(d)].

Figures 3(a) and 3(b) show the quasienergy band structures of Hermitian ($\gamma = 0$) and non-Hermitian ($\gamma = 0.005k_0$) waveguide arrays under OBCs of $N = 60$, which are calculated by coupled mode theory (CMT) [54]. According to the Floquet theory, each replica band consists of 60 modes. Here only ten modes around $\varepsilon = \omega/2$ are shown for better visualization. It is evident that the Hermitian system only supports bulk modes, corresponding to the topologically trivial phase [Fig. 3(a)]. However, the π gap reopens when the system is driven to the topological nontrivial phase by a certain amount of gain and loss, and two discrete modes emerge inside the π gap (i.e., the π modes) [Fig. 3(b)]. The inset shows the imaginary part of quasienergy, indicating that one of the π modes is the gain mode (red) while the other is lossy (blue). The mode intensity profiles at $z = 0$ (the initial stage) of these two topological states (circled by red dotted box) are shown in Fig. 3(c). The topological gain mode mainly locates on the first gain waveguide and the lossy mode locates on the last lossy one. These two π modes propagate with periodically oscillated fields across the first three waveguides around the boundary, as shown in Fig. 3(d). It is clear that the optical field mainly locates on the first waveguide at the beginning and switches to the third one at the middle of one period (see Appendix A for detailed Floquet theory analysis).

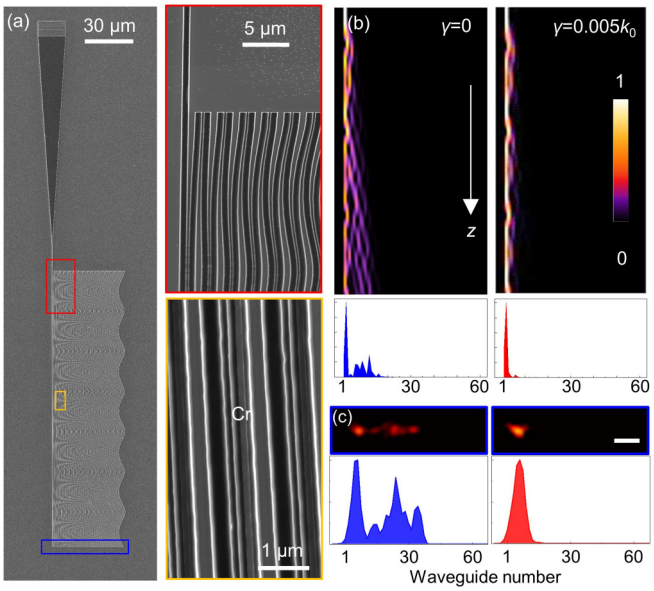

FIG. 4. (a) SEM image and enlarged regions of the non-Hermitian sample. Left: Full view of the sample, consisting of a grating coupler, a taper, and the waveguide array. Right top: Input waveguide. Right bottom: Cr on the waveguide. (b) CMT calculated optical field propagation in Hermitian (left) and non-Hermitian (right) waveguide arrays and corresponding normalized output intensities (bottom). (c) Experimental detected output intensities of Hermitian (left) and non-Hermitian (right) sample. Top: CCD recorded output signal. Bottom: Output intensities, which are normalized to maximum. Scale bar = 10 μm.

To confirm the non-Hermiticity-induced Floquet π modes, we then investigate the dynamics of light with single waveguide excitation at the boundary for considering systems both theoretically and experimentally. Figure 4(b) shows theoretical (CMT) calculated optical field evolutions of different systems for 60 waveguides and 200-μm propagations. Note that the field intensity was normalized at every distance z for better visualization. It is clearly observed that the field penetrates into the bulk as it propagates within the waveguide array for the Hermitian case, since the system is in the trivial phase of the low frequency region. As a certain gain/loss ($\gamma = 0.005k_0$) is introduced to reach a nontrivial phase, the localized π modes can be excited with the field confined along the edge without spreading into the bulk. The extracted field intensities from the output at $z = 200\,\mu$m are shown at the bottom of Fig. 4(b). The optical field is strongly localized (around 90% energy locates on the first three waveguides) in the non-Hermitian waveguides array according to the excitation of the π mode, while for the Hermitian waveguide array a majority of energy (~60%) penetrates into the bulk.

Afterwards, experiments were carried out based on the passive PT symmetric [51,54,57] configuration in a silicon waveguide platform. The waveguide width (w) and height (h) are optimized as $w = 400$ nm and $h = 220$ nm, in which only one fundamental mode is supported at $\lambda = 1550$ nm with propagation constant $\beta_0 = 2.1601k_0$. The waveguide bending profile is carefully designed so that the coupling coefficients satisfy $c_0 = 0.02k_0$, $\delta_0 = 0.015k_0$ and $\omega = 1.33c_0$ (see Appendix B). The loss modulation is introduced by depositing lossy metal (i.e., chrome) stripes on top of every other silicon waveguide, where the loss is engineered by the width of the Cr strip (see Appendix C) [54]. Here, a 100-nm-wide and 2-nm-thick chrome (Cr) layer is applied, corresponding to the loss modulation $2\gamma = 0.01k_0$. The experimental samples are fabricated by E-beam lithography and the inductively coupled plasma (ICP) etching process (see Appendix C), which include the waveguide array (60 waveguides with 200 μm length, the same as the CMT calculations) and input grating coupler that is connected to the edge waveguide [see the scanning electron microscopy (SEM) images in Fig. 4(a)]. In experiment, the light was input into the waveguide lattice by focusing the laser ($\lambda = 1550$ nm) via an input grating coupler. The transmitted signals were collected directly from the scattered light from the output by a near-infrared charge-coupled device (CCD) camera. The field intensity distribution at output ends are captured by a CCD camera with the intensities plotted out, as shown in Fig. 4(c). In the Hermitian waveguide array diffraction into the bulk of the lattice occurs, while as the loss is introduced ($2\gamma = 0.01k_0$) the bulk diffraction is suppressed and the topological π modes form. The experimental results are in good agreement with the CMT calculations. It is evident that this non-Hermitian system hosts the localized π mode and this nontrivial Floquet state supports localized energy transport.

So far, we have demonstrated the recovery of the π mode by non-Hermitian modulation. It is due to the fact that the coupling between different replicas can be drastically modulated by non-Hermitian gain/loss, which can reopen the π gap for an initially nongapped topological trivial system. Note that the non-Hermiticity can lead to mode degeneracy, which has been utilized to achieve zero mode recovery in static SSH models [54]. In contrast to that effect, we show here that non-Hermiticity can compress replica bands in Floquet systems and construct the π band gap, thus recovering the topological π mode. Besides, we noticed that there are several reported works investigating the Floquet non-Hermitian system [44,58,59], and these works focus on the non-Hermitian skin effect. We want to address that the skin effect, which leads to mode localization on the boundary and breaks the bulk-edge correspondence, is not relevant in our work, since our system does not contain asymmetric coupling, which is required by skin effect.

In conclusion, we have successfully demonstrated the recovery of the Floquet π mode in a periodically driven non-Hermitian SSH model by tuning the loss. The topological phase diagram clearly shows the Floquet topological transition modulated by PT symmetric gain and loss, ensuring the emergence of the topologically protected π mode. The recovered π mode shows good localization on the edge and supports robust transport. The experimental results in silicon waveguides with controlled loss are consistent with the theoretical prediction. Our results show that the topological nature of a Floquet system can be manipulated by non-Hermitian engineering, which would inspire more insightful explorations in topological and PT photonics.

The authors thank Y. Pan, Q. Cheng, and H. Wang for helpful discussions. This work was supported by the National

Key R&D Program of China (Grants No. 2017YFA0303701 and No. 2016YFA0202103) and the National Natural Science Foundation of China (Grants No. 91850204 and No. 11674167). T.L. acknowledges the support from Dengfeng Project B of Nanjing University.

APPENDIX A: FLOQUET MODE

For the curved waveguide array, Floquet theory provides a framework for treating this time-periodic Hamiltonian $H(t+P)=H(t)$ with a period $P=2\pi/\omega$. According to this theory, the solution of the Schrödinger equation can be written as a superposition of Floquet states:

$$|\psi_\alpha(t)\rangle = \exp(-i\varepsilon_\alpha t)|u_\alpha(t)\rangle, \tag{A1}$$

where ε_α is the quasienergy and $|u_\alpha(t)\rangle$ is the associated Floquet mode. The quasienergies are defined up to integer multiplies of ω, and the Floquet modes are P-periodic functions $|u_\alpha(t+P)\rangle = |u_\alpha(t)\rangle$ and they belong to the extended Hilbert space, a direct product of the usual Hilbert space and the space of time-periodic functions with period $P=2\pi/\omega$. By substituting the Floquet ansatz (A1) into the Schrödinger equation, we can obtain an eigenvalue equation

$$\left(H(t)-i\frac{\partial}{\partial t}\right)|u_\alpha(t)\rangle = \varepsilon_\alpha|u_\alpha(t)\rangle. \tag{A2}$$

Using the spectral decomposition of the Hamiltonian and the Floquet modes,

$$H(t) = \sum_{n=-\infty}^{\infty} e^{-in\omega t}H_n,$$
$$|u_\alpha(t)\rangle = \sum_{n=-\infty}^{\infty} e^{-in\omega t}\left|u_\alpha^n\right\rangle, \tag{A3}$$

we arrive at the time-independent Floquet equation:

$$(H_0-n\omega)\left|u_\alpha^n\right\rangle + \sum_{m\neq 0} H_m\left|u_\alpha^{n-m}\right\rangle = \varepsilon_\alpha\left|u_\alpha^n\right\rangle, \quad \forall n\in\mathbb{Z}. \tag{A4}$$

Then we apply the Floquet approach to our periodically curved waveguide array system. The corresponding Hamiltonian can be written as a sum of time-independent and time-periodic parts,

$$H(t) = H_0 + H_p(t), \tag{A5}$$

where

$$H_0 = \sum_{n=1}^{N-1}[\beta_0-(-1)^n i\gamma]c_n^\dagger c_n + \sum_{n=1}^{N-1} c_0 c_n^\dagger c_{n+1} + \text{H.c.} \tag{A6}$$

and

$$H_p(t) = \sum_{n=1}^{N-1}(-1)^n\delta_0\cos(\omega t)c_n^\dagger c_{n+1} + \text{H.c.} \tag{A7}$$

In further calculations, we express H_0 and H_p as $N\times N$ matrices

$$H_0 = \begin{pmatrix} i\gamma & c_0 & 0 & \cdots \\ c_0 & -i\gamma & c_0 & \\ 0 & c_0 & i\gamma & \\ & \vdots & & \ddots \end{pmatrix}_{N\times N} \tag{A8}$$

and

$$H_p(t) = H_1 e^{-i\omega t} + H_{-1}e^{i\omega t}. \tag{A9}$$

Note that we set the propagation constant β_0 to zero as a reference value. The Fourier components $H_{\pm1}$ are represented by

$$H_{\pm1} = \frac{1}{2}\begin{pmatrix} 0 & -\delta_0 & 0 & \cdots \\ -\delta_0 & 0 & \delta_0 & \\ 0 & \delta_0 & 0 & \\ & \vdots & & \ddots \end{pmatrix}_{N\times N}. \tag{A10}$$

Then the time-independent Floquet equation (A4) can be represented as the following eigenvalue problem with a block-matrix operator:

$$\begin{pmatrix} \ddots & & & & \\ H_1 & H_0+\omega & H_{-1} & & \\ & H_1 & H_0 & H_{-1} & \\ & & H_1 & H_0-\omega & H_{-1} \\ & & & & \ddots \end{pmatrix}\begin{pmatrix} \vdots \\ u_\alpha^{-1} \\ u_\alpha^0 \\ u_\alpha^1 \\ \vdots \end{pmatrix}$$
$$= \varepsilon_\alpha\begin{pmatrix} \vdots \\ u_\alpha^{-1} \\ u_\alpha^0 \\ u_\alpha^1 \\ \vdots \end{pmatrix}. \tag{A11}$$

This equation reveals an interpretation of the Floquet approach: it transforms a 1D time-periodic problem to a 2D time-independent problem where the Floquet replicas build up a synthetic dimension [23,27,60,61].

By truncating Eq. (A11) at a sufficiently large n, we can get the eigenvectors and eigenvalues that converge well. The corresponding eigenvectors contain the Fourier components of the Floquet modes $|u_\alpha^n\rangle$, where each of them is associated with the energy $\varepsilon_\alpha^n = \varepsilon_n + n\omega$. The solution of the Schrödinger equation is given by

$$|\Psi(t)\rangle = \sum_\alpha C_\alpha \sum_n \exp\left(-i\varepsilon_\alpha^n t\right)\left|u_\alpha^n\right\rangle, \tag{A12}$$

where the constants $C_\alpha = \langle u_\alpha(0)|\Psi(0)\rangle$ are determined by the initial condition $|\Psi(0)\rangle$.

We investigated the Floquet modes in the waveguide array of $N=60$. By truncating the replica at $n=3$, we theoretically calculated the propagation properties of Floquet modes, and the evolution of the PT recovered π mode in one period is shown in Fig. 3(d). The quasienergy of the two modes have a nonzero imaginary part, and one is a gain mode and another is a lossy mode, shown in Fig. 3(d) left and right, respectively. These two modes show a good localization property and mainly propagate along the boundary. Another important property is that these two modes periodically oscillate among

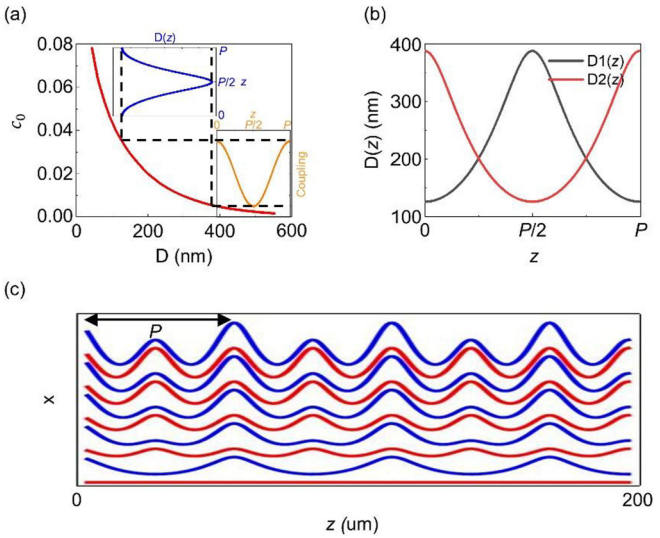

FIG. 5. (a) Coupling coefficient under different waveguide gaps (edge to edge). The coupling strength does not depend on the gap linearly. Inset shows the inverse designed gap from the relation between gap and coupling strength. (b) $D(z)$ of adjacent waveguides for cosine coupling modulation. $D1(z)$ and $D2(z)$ correspond to $c_0 + \delta(z)$ and $c_0 - \delta(z)$ respectively. (c) Scheme of designed waveguide array. Only ten waveguides are plotted.

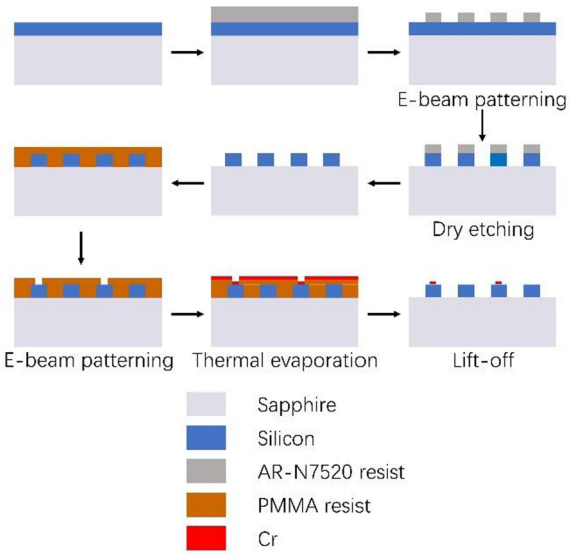

FIG. 6. Fabrication flow of the photonic silicon waveguide array deposited with Cr.

the three waveguides on the edge. It is clear that they mainly locate on the first waveguide at the beginning and end of one period and locate on the third one at the middle of one period.

APPENDIX B: WAVEGUIDE DESIGN

The waveguide modes in two adjacent waveguides couple to each other due to filed overlap, and the coupling coefficient depends on the field overlap integration. Figure 5(a) shows the coupling coefficient of two guide modes at different gaps between the two waveguides, indicating the coupling strength depends exponentially on the separation between adjacent waveguides. In order to realize the sinusoidal coupling modulation, the gap between adjacent waveguides is carefully designed, as shown in the insets in Figs. 5(a) and 5(b). The gap is inverse designed from the dependence of coupling strength on the gap so that the designed waveguide profile matches the exact sinusoidal coupling modulation. $D1(z)$ and $D2(z)$ correspond to $c_0 + \delta(z)$ and $c_0 - \delta(z)$ respectively. Only one Floquet period is plotted. Figure 5(c) shows the scheme of a periodically curved waveguide array of 200 μm.

APPENDIX C: FABRICATION OF THE PHOTONICS SILICON WAVEGUIDE ARRAY DEPOSITED WITH CHROMIUM (Cr)

The experimental samples were fabricated using the method of electron beam lithography (EBL) and the dry etching process, which is followed by a second-step E-beam lithography with the alignment and lift-off process to deposit the Cr stripes. Figure 6 shows the fabrication flow and sample schematics of each step, respectively. The substrate used here is 460-μm alumina substrate with 220-nm silicon deposition. The substrates were cleaned in an ultrasound bath in acetone, isopropyl alcohol (IPA), and DI water for 15 min respectively and dried under clean nitrogen flow. The alignment marks were then patterned by EBL (Elionix, ELS-F125), deposition of chromium/gold (5 nm/40 nm) layers, and photoresist liftoff (see Fig. 6). After that, the waveguide arrays and grating nanostructures were exposed to EBL. The samples were then used to dry etch the silicon layer in a 2:5 mixture of SF6 and C4F8 plasma and the residual photoresist was stripped off by an oxygen plasma stripper. Next, the chromium structures were fabricated by an alignment E-beam lithography and lift-off process. The photoresist film was spin coated onto the substrate. After exposing the structure, 2-nm chromium film is deposited using thermal evaporation, then removing the photoresist by soaking in N-methyl-2-pyrrolidone.

APPENDIX D: IMAGINARY PART OF THE QUASIENERGY SPECTRUM

The quasienergy of Floquet modes in the non-Hermitian case become complex due to the induced gain and loss. The imaginary part of the spectrum is shown in Fig. 7, and the highlighted red curves correspond to Floquet π modes. The absolute values of the imaginary part of the quasienergy of the π modes increase due to the increasing gain/loss strength. Further increasing γ leads to better localization of the π modes, and as a result, the absolute values of the imaginary part decrease [40].

APPENDIX E: TOPOLOGICAL ANALYSIS

The topological invariant G_π of the considered Floquet system is defined based on the time evolution operator. The time evolution operator is $U(z, z_0) = \hat{T} e^{\int_{z_0}^{z} H(z')dz'}$, where $\hat{T}$ is the time-ordering operator. Without loss of generality, we can simplify $U(z, z_0)$ to $U(z)$ by setting $z_0 = 0$. The time-averaged effective Hamiltonian is $H_F = (i/P) \ln U(P)$. According to Bloch theory, $U(z)$ and H_F can be decomposed as $U(z) = \Pi U(z, k)$ and $H_F = \Sigma_k H_F(k)$. The Z-valued

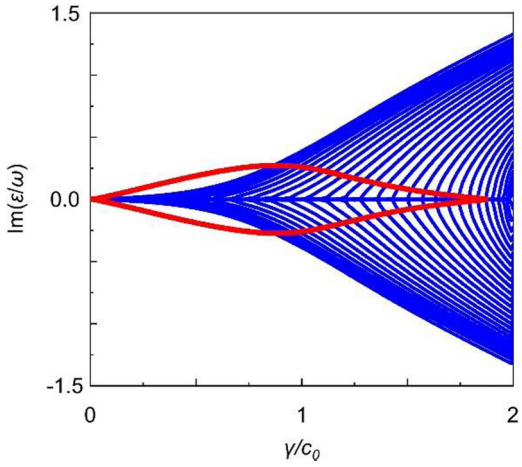

FIG. 7. Imaginary part of quasienergy spectrum with increasing gain/loss strength γ. The Floquet frequency is set to $\omega = 1.33c_0$.

invariant G_π can be defined for a gap at π for a Floquet system with chiral symmetry, which applies precisely to our system in the Hermitian case $[\sigma_z H(z,k)\sigma_z = -H(-z,k)]$,

$$G_\pi = \frac{i}{2\pi}\int_{-\pi}^{\pi} \mathrm{tr}[(V_\pi^+)^{-1}\partial_k V_\pi^+]dk. \tag{E1}$$

The V_π^+ is obtained from $V(z,k)$ at half period, defined as

$$V(z,k) = U(z,k)e^{iH_F(k)z}, \tag{E2}$$

$$V\left(\frac{P}{2},k\right) = \begin{pmatrix} V_\pi^+ & 0 \\ 0 & V_\pi^- \end{pmatrix}. \tag{E3}$$

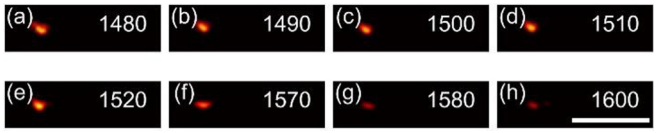

FIG. 8. Experimentally captured output signals with different wavelengths. (a)–(h) Correspond to $\lambda = 1480$, 1490, 1500, 1510, 1520, 1570, 1580, and 1600 nm, respectively. Scale bar $= 30\ \mu$m.

APPENDIX F: EXPERIMENTAL RESUILTS OF BROADBAND CHARACTERIZATION

The recovered π mode lies in the Floquet π gap, thus it is robust to a certain amount of perturbations on the coupling coefficients. Since the coupling coefficients between adjacent waveguides depend on the wavelength, the recovered π mode should exist in a broadband spectrum [62]. To verify this, further experiments were performed on the non-Hermitian Floquet waveguide lattice with respect to different wavelengths, and the results are shown in Fig. 8. We changed the incident wavelength (from 1480 to 1600 nm), and collected the scattered light at the output of waveguide lattice by a CCD camera. It is clear that the localization of output light on the first waveguide persists in the wavelength range 1400–1600 nm, thus verifying the broadband property of the recovered π mode. The decrease of output intensity at longer wavelength is due to the coupling efficiency of the grating coupler.

[1] W. P. Su, J. R. Schrieffer, and A. J. Heeger, Solitons in Polyacetylene, Phys. Rev. Lett. **42**, 1698 (1979).

[2] C. Poli, M. Bellec, U. Kuhl, F. Mortessagne, and H. Schomerus, Selective enhancement of topologically induced interfaces states in a dielectric resonator, Nat. Commun. **6**, 6710 (2015).

[3] Q. Cheng, Y. Pan, Q. Wang, T. Li, and S. Zhu, Topologically protected interface mode in plasmonic waveguide arrays, Laser Photon. Rev. **9**, 392 (2015).

[4] H. Zhao, P. Miao, M. H. Teimourpour, S. Malzard, R. El-Ganainy, H. Schomerus, and L. Feng, Topological hybrid silicon microlasers, Nat. Commun. **9**, 981 (2018).

[5] Y. Wang, Y. Lu, F. Mei, J. Gao, Z. Li, H. Tang, S. Zhu, S. Jia, and X. Jin, Direct Observation of Topology from Single-Photon Dynamics, Phys. Rev. Lett. **122**, 193903 (2019).

[6] P. St-Jean, V. Goblot, E. Galopin, A. Lemaitre, T. Ozawa, L. Le Gratiet, I. Sagnes, J. Bloch, and A. Amo, Lasing in topological edge states of a one-dimensional lattice, Nat. Photon. **11**, 651 (2017).

[7] M. Parto, S. Wittek, H. Hodaei, G. Harari, M. A. Bandres, J. Ren, and M. C. Rechtsman, Edge-Mode Lasing in 1D Topological Active Arrays, Phys. Rev. Lett. **120**, 113901 (2018).

[8] W. Song, W. Sun, C. Chen, Q. Song, S. Xiao, S. Zhu, and T. Li, Robust and broadband optical coupling by topological waveguide arrays, Laser Photon. Rev. **14**, 1900193 (2020).

[9] G. E. Topp, N. Tancogne-Dejean, A. F. Kemper, A. Rubio, and M. A. Sentef, All-optical nonequilibrium pathway to stabilizing magnetic Weyl semimetals in pyrochlore iridates, Nat. Commun. **9**, 4452 (2018).

[10] T. Oka and H. Aoki, Photovoltaic Hall effect in graphene, Phys. Rev. B **79**, 081406(R) (2009).

[11] J. W. Mclver, B. Schulte, F.-U. Stein, T. Matsuyama, G. Meier, and A. Cavalleri, Light-induced anomalous Hall effect in graphene, Nat. Phys. **16**, 38 (2020).

[12] H. Hübener, M. A. Sentef, U. De Giovannini, A. F. Kemper, and A. Rubio, Creating stable Floquet-Weyl semimetals by laser-driving of 3D Dirac materials, Nat. Commun. **8**, 13940 (2017).

[13] G. Jotzu, M. Messer, R. Desbuquois, M. Lebrat, T. Uehlinger, D. Greif, and T. Esslinger, Experimental realization of the topological Haldane model with ultracold fermions, Nature (London) **515**, 237 (2014).

[14] A. Eckardt, Colloquium: Atomic quantum gases in periodically driven optical lattices, Rev. Mod. Phys. **89**, 011004 (2017).

[15] I. L. Garanovich, S. Longhi, A. A. Sukhorukov, and Y. S. Kivshar, Light propagation and localization in modulated photonic lattices and waveguides, Phys. Rep. **518**, 1 (2012).

[16] S. Longhi and K. Staliunas, Self-collimation and self-imaging effects in modulated waveguide arrays, Opt. Commun. **281**, 4343 (2008).

[17] S. Longhi, Self-imaging and modulational instability in an array of periodically curved waveguides, Opt. Lett. **30**, 2137 (2005).

[18] S. Longhi, D. Janner, M. Marano, and P. Laporta, Quantum-mechanical analogy of beam propagation in waveguides with a

bent axis: Dynamic-mode stabilization and radiation-loss suppression, Phys. Rev. E **67**, 036601 (2003).

[19] M. Holthaus, Floquet engineering with quasienergy bands of periodically driven optical lattices, J. Phys. B **49**, 013001 (2016).

[20] B. Zhu, H. Zhong, Y. Ke, X. Qin, A. A. Sukhorukov, Y. S. Kivshar, and C. Lee, Topological Floquet edge states in periodically curved waveguides, Phys. Rev. A **98**, 013855 (2018).

[21] M. C. Rechtsman, J. M. Zeuner, Y. Plotnik, Y. Lumer, D. Podolsky, F. Dreisow, S. Nolte, M. Segev, and A. Szameit, Photonic Floquet topological insulators, Nature (London) **496**, 196 (2013).

[22] J. K. Asbóth, B. Tarasinski, and P. Delplace, Chiral symmetry and bulk-boundary correspondence in periodically driven one-dimensional systems, Phys. Rev. B **90**, 125143 (2014).

[23] V. Dal Lago, M. Atala, and L. E. F. Foa Torres, Floquet topological transitions in a driven one-dimensional topological insulator, Phys. Rev. A **92**, 023624 (2015).

[24] M. Fruchart, Complex classes of periodically driven topological lattice systems, Phys. Rev. B **93**, 115429 (2016).

[25] Q. Cheng, Y. Pan, H. Wang, C. Zhang, D. Yu, A. Gover, H. Zhang, T. Li, L. Zhou, and S. Zhu, Observation of Anomalous pi Modes in Photonic Floquet Engineering, Phys. Rev. Lett. **122**, 173901 (2019).

[26] W. Song, H. Li, S. Gao, C. Chen, S. Zhu, and T. Li, Subwavelength self-imaging in cascaded waveguide arrays, Adv. Photon. **2**, 036001 (2020).

[27] Z. Fedorova, C. Jörg, C. Dauer, F. Letscher, M. Fleischhauer, S. Eggert, S. Linden, and G. von Freymann, Limits of topological protection under local periodic driving, Light. Sci. Appl. **8**, 63 (2019).

[28] J. Petráček and V. Kuzmiak, Dynamics and transport properties of Floquet topological edge modes in coupled photonic waveguides, Phys. Rev. A **101**, 033805 (2020).

[29] W. Song, H. Li, S. Gao, S. Wu, C. Chen, S. Zhu, and T. Li, Gauge-induced Floquet topological states in photonic waveguides, arXiv:2010.05408.

[30] Y. Yu, Y. Song, T. Chen, H. Wang, S. Zhuang, and Q. Chen, Floquet spectrum and optical behaviors in dynamic Su–Schrieffer–Heeger modeled waveguide array, Chin. Opt. Lett. **19**, 042601 (2021).

[31] H. Hodaei, A. U. Hassan, S. Wittek, H. Garcia-Gracia, R. El-Ganainy, and D. N. Christodoulides, Enhanced sensitivity at higher-order exceptional points, Nature (London) **548**, 187 (2017).

[32] W. Chen, S. K. Özdemir, G. Zhao, J. Wiersig, and L. Yang, Exceptional points enhance sensing in an optical microcavity, Nature (London) **548**, 192 (2017).

[33] L. Feng, Z. J. Wong, R.-M. Ma, Y. Wang, and X. Zhang, Single-mode laser by parity-time symmetry breaking, Science **346**, 972 (2014).

[34] H. Hodaei, M.-A. Miri, M. Heinrich, D. N. Christodoulides, and M. Khajavikhan, Parity-time–symmetric microring lasers, Science **346**, 975 (2014).

[35] S. Longhi, PT-symmetric laser absorber, Phys. Rev. A **82**, 031801 (2010).

[36] L. Ge, Y. D. Chong, S. Rotter, H. E. Türeci, and A. D. Stone, Unconventional modes in lasers with spatially varying gain and loss, Phys. Rev. A **84**, 023820 (2011).

[37] Y. D. Chong, L. Ge, and A. D. Stone, PT-Symmetry Breaking and Laser-Absorber Modes in Optical Scattering Systems, Phys. Rev. Lett. **106**, 093902 (2011).

[38] L. Feng, Y.-L. Xu, W. S. Fegadolli, M.-H. Lu, J. E. B. Oliveira, V. R. Almeida, Y.-F. Chen, and A. Scherer, Experimental demonstration of a unidirectional reflectionless parity-time metamaterial at optical frequencies, Nat. Mater. **12**, 108 (2013).

[39] Z. Lin, H. Ramezani, T. Eichelkraut, T. Kottos, H. Cao, and D. N. Christodoulides, Unidirectional Invisibility Induced by PT-Symmetric Periodic Structures, Phys. Rev. Lett. **106**, 213901 (2011).

[40] A. Guo, G. J. Salamo, D. Duchesne, R. Morandotti, M. Volatier-Ravat, V. Aimez, G. A. Siviloglou, and D. N. Christodoulides, Observation of PT-Symmetry Breaking in Complex Optical Potentials, Phys. Rev. Lett. **103**, 093902 (2009).

[41] K. Takata and M. Notomi, Photonic Topological Insulating Phase Induced Solely by Gain and Loss, Phys. Rev. Lett. **121**, 213902 (2018).

[42] Z. Turker, S. Tombuloglu, and C. Yuce, PT symmetric Floquet topological phase in SSH model, Phys. Lett. A **382**, 2013 (2018).

[43] L. Zhou, Dynamical characterization of non-Hermitian Floquet topological phases in one dimension, Phys. Rev. B **100**, 184314 (2019).

[44] H. Wu and J.-H. An, Floquet topological phases of non-Hermitian systems, Phys. Rev. B **102**, 041119(R) (2020).

[45] L. Zhou and J. Gong, Non-Hermitian Floquet topological phases with arbitrarily many real-quasienergy edge states, Phys. Rev. B **98**, 205417 (2018).

[46] X. Zhang and J. Gong, Non-Hermitian Floquet topological phases: Exceptional points, coalescent edge modes, and the skin effect, Phys. Rev. B **101**, 045415 (2020).

[47] C. Yuce, PT symmetric Floquet topological phase, Eur. Phys. J. D **69**, 184 (2015).

[48] D. Kim, K. Mochizuki, N. Kawakami, and H. Obuse, Bulk-edge correspondence in nonunitary Floquet systems with chiral symmetry, Phys. Rev. A **102**, 062202 (2020).

[49] A. K. Hater and N. Hatano, Real edge modes in a Floquet-modulated PT-symmetric SSH model, arXiv:2006.16890.

[50] Y. Yu, W. Song, C. Chen, T. Chen, H. Ye, X. Shen, Q. Cheng, and T. Li, Phase transition of non-Hermitian topological edge states in microwave regime, Appl. Phys. Lett. **116**, 211104 (2020).

[51] S. Weimann, M. Kremer, Y. Plotnik, Y. Lumer, S. Nolte, K. G. Makris, M. Segev, M. C. Rechtsman, and A. Szameit, Topologically protected bound states in photonic parity-time-symmetric crystals, Nat. Mater. **16**, 433 (2017).

[52] L. Zhou, Non-Hermitian Floquet topological superconductors with multiple Majorana edge modes, Phys. Rev. B **101**, 014306 (2020).

[53] L. Zhou, Y. Gu, and J. Gong, Dual topological characterization of non-Hermitian Floquet phases, Phys. Rev. B **103**, L041404 (2021).

[54] W. Song, W. Sun, C. Chen, Q. Song, S. Xiao, S. Zhu, and T. Li, Breakup and Recovery of Topological Zero Modes in Finite Non-Hermitian Optical Lattices, Phys. Rev. Lett. **123**, 165701 (2019).

[55] H. Zhao, X. Qiao, T. Wu, B. Midya, S. Longhi, and L. Feng, Non-Hermitian topological light steering, Science **365**, 1163 (2019).

[56] Z. Fedorova, H. Qiu, S. Linden, and J. Kroha, Observation of topological transport quantization by dissipation in fast Thouless pumps, Nat. Commun. **11**, 3758 (2020).

[57] Y. N. Joglekar and A. K. Harter, Passive parity-time-symmetry-breaking transitions without exceptional points in dissipative photonic systems, Photon. Res. **6**, A51 (2018).

[58] B. Höckendorf, A. Alvermann, and H. Fehske, Topological origin of quantized transport in non-Hermitian Floquet chains, Phys. Rev. Research **2**, 023235 (2020).

[59] Y. Cao, Y. Li, and X. Yang, Non-Hermitian bulk-boundary correspondence in a periodically driven system, Phys. Rev. B **103**, 075126 (2021).

[60] D. Thuberg, S. A. Reyes, and S. Eggert, Scaling behavior of quantum critical relaxation dynamics of a system in a heat bath, Phys. Rev. B **93**, 180301(R) (2016).

[61] S. A. Reyes, D. Thuberg, D. Perez, C. Dauer, and S. Eggert, Transport through an AC-driven impurity: Fano interference and bound states in the continuum, New J. Phys. **19**, 043029 (2017).

[62] A. Redondo, I. Andonegui, M. Collins, G. Harari, Y. Lumer, M. Rechtsman, B. Eggleton, and M. Segev, Topological Optical Waveguiding in Silicon and the Transition between Topological and Trivial Defect States, Phys. Rev. Lett. **116**, 163901 (2016).